# Active Control of Robot Structure Deflections

**A. Zalucky**

**D. E. Hardt**

Laboratory for Manufacturing and Productivity, Massachusetts Institute of Technology, Cambridge, Mass. 02139

*The characteristic beam-like structure of most robots leads to significant bending deflections, which in turn lead to poor endpoint positioning accuracy. One solution is to actively counteract this bending using a "straightness servo." In this paper, such a system is proposed comprising two parallel beams, one to act as the manipulator link and one to carry only the bending loads. These beams are clamped together at one end and joined at the other by an hydraulic actuator. A single variable straightness control system is presented and analyzed. Simulations based upon a realistically sized prototype indicate that attenuation of force disturbances (compliance reduction) to less than 0.006 cm/kN (e.g., 0.001 in./100 lb.) is possible over a 10 Hz bandwidth. Also, system stability can be maintained even when additional mass (which changes the system parameters) is placed at the endpoint. There results are verified by experiments on a full size prototype. Greater improvements in system bandwidth will require state variable control because of the high dynamic order of the structure.*

## Introduction

The lack of positioning accuracy in current industrial manipulators limits application to tasks that are error tolerant, such as pick and place or painting operations, or to tasks where a passive compliant element can be used to correct for these errors. It clearly also limits the load capacity of these devices to levels well below their structural or drive system limits. These errors arise from several sources such as structural deflections (both static and dynamic), wear, and drive system friction and backlash. As a result, these errors are not only persistent, they change with time and are often random in appearance.

Most manufacturing and many assembly tasks require position tolerances on the order of 0.025 mm (0.001 in.), yet sufficiently robust industrial manipulators with large working envelopes are characterized by repeatable positioning with a 0.25 mm envelope. Functions requiring high accuracy and stiffness include simple machining operations such as drilling, trimming, routing, detailled deburring and some fastening operations such as riveting or screw fastening. Since no commercially available robots have sufficient stiffness or accuracy to perform such tasks, implementation of these operations, such as that demonstrated by General Dynamics [1] have had to redefine the task and use both added passive compliance and large templates of complex shape. As a result, cost and flexibility improvements through automation were partly offset by an increased cost of task preparation.

There has been little work in the area of precision manipulation, and it is clear that without a change in direction such a label will remain a contradiction in terms. A state of the art robot today remains a "sloppy NC machine" and, as Book [2] points out, this must be so since weight and stiffness are inversly related to bandwidth and range of movement. Therefore, precise manipulation is now achieved by constructing massive structural members (and the device becomes a machine tool), while lighter more resonant structures are used when wide range and high speed (but low accuracy) movement is required.

One solution to this problem is to make a full kinematic state measurement at the endpoint of the manipulator and use the resulting error signal to correct the position and orientation of the end effector. By using such a measurement, all deflections, backlash, and other error producing realities of the manipulator are lumped into one set of measured variables. This method depends upon the use of end effector position measurements in an absolute reference frame (not linked to the manipulator structure), that provide an uncorruptable error signal upon which the maniuplator controller can act.

However, endpoint feedback is difficult because high accuracy three-dimiensional position and orientation measurements must be made over a large operating volume. Also, the requirements on the error-nulling micromanipulator are severe with respect to weight, bandwidth and force. Accordingly, this paper addresses a different approach to this problem of precision manipulation that concentrates on errors caused by structural deflections.

## Link Deflection Compensation

A typical robotic manipulator for general industrial application (whether articular or cartesian) has at least one or more beam-like links. This linked structure provides the wide range of motion characteristic of industrial robots, but also causes the basic structure to be inherently low in stiffness. If

Contributed by the Dynamic Systems and Control Division for publication in the JOURNAL OF DYNAMIC SYSTEMS, MEASUREMENT, AND CONTROL. Manuscript received by the Dynamic Systems and Control Division, June 7, 1982.

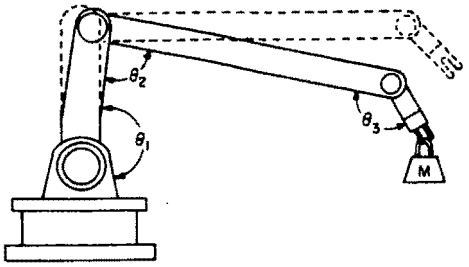


Fig. 1 Endpoint error with correct joint angles

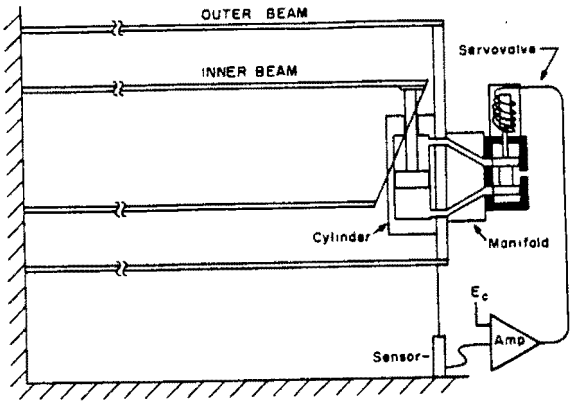


Fig. 2 Basic system

each link is considered a simple cantilever beam, as is the case with articular robots, it can be seen that the major cause of large deflections is bending.

These bending deflections, as shown in Fig. 1, are caused by both the load of the structure itself and any forces at the endpoint, and can lead to significant positioning errors even when joint servos are perfectly accurate and stiff to torque disturbances. Thus if the beams can be made stiff to bending loads without a significant increase in size or weight, the major source of error can be eliminated.

A system to accomplish this is shown in Fig. 2. Essentially two cantilever beams in parallel, the outer beam is the manipulator link while the inner beam acts as the actual bending load carrying member. Any bending in the outer beam is sensed by a straightness measurement (see for example Fig. 3) and the load is transferred to the inner beam via the force actuator. Thus a beam-straightness servo or active stiffness controller is created to actively maintain the endpoint position of the outer beam at a fixed value regardless of load disturbances. The outer beam still carries applied moments, but the resulting rotation can be shown to be quite small with respect to the deflections caused by end forces for a given beam section.

It should be noted that this problem and solution is not unlike that of active beam vibration damping. However, there is a major difference here in that static as well as unknown dynamic force distrubances must be rejected. Therefore solutions such as described in [4] are not applicable here.

## System Design and Modelling

The dynamic system that results from the active coupling of two cantilevered beams is quite complex, even when only first modes of vibration are considered; and as will be shown, the disturbance response of this system is highly dependent upon the relative parameter values describing the basic structure. Accordingly it was decided to first develop a prototype design based on realistic dimensions and loads for an industrial manipulator, and use this design as a basis for evaluating this concept.

For simplicity and ease of construction, only one bending

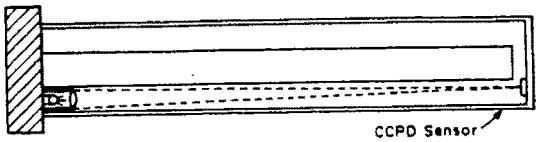


Fig. 3 Optical displacement sensor

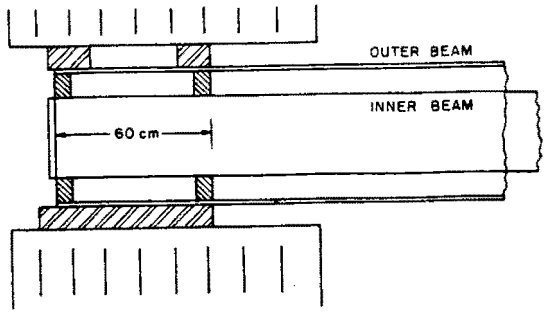


Fig. 4 Base mounting method

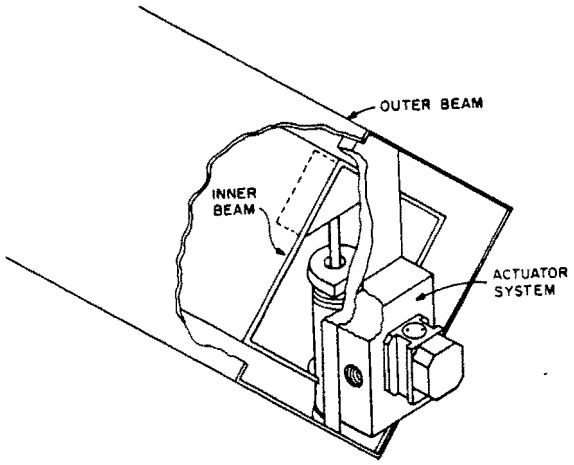


Fig. 5 Prototype system

axis was considered thus allowing load disturbance rejection in only one perpendicular direction. Another simplification in the prototype was the measurement transducer, which was an externally supported displacement transducer rather than a beam straightness measurement (see Fig. 2).

The prototype was sized to accommodate loads of up to 2000 N a figure large enough to encompass the capability of any large modern robot. The design described in [5], involved an optimization procedure where weight was minimized subject to beam strength and inner-outer beam clearance constraints. This resulted in the following specifications and components:

- one 1.5 meter long 140 × 140 × 2.3 mm square channel aluminum beam used as the outer beam
- one 1.5 meter 100 × 100 × 3.2 mm square channel aluminum beam used as the inner beam
- one 12.7 mm diameter double-acting, single-ended hydraulic cylinder
- one high-speed proportional 4-way flow control servovalve (Moog, Inc., type 30)
- a servoamplifier
- a 20 MPa (3000 psi) hydraulic power supply
- a DCDT position transducer

The smaller beam was placed within the larger, spacers were inserted, and the two beams were mounted in a rigid base as shown in Fig. 4. The actuator module consisting of the cylinder, valve, and manifold mounted on a support, was then installed at the free end (see Fig. 5). The DCDT was

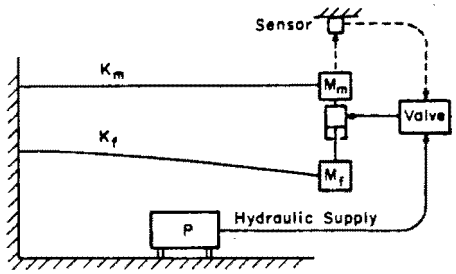


Fig. 6 System with lumped mass beams

positioned to measure vertical deflection of the outer beam and its output fed back to the servoamplifier.

## System Model

The basic components of the prototype are shown in Fig. 2. Included in Fig. 2 is a control input to the servoamp, $E_c$. In the analysis of disturbance force rejection, this input is assumed to be zero at all times. (Note that the control inut, where nonzero, may also be used to actively position the outer beam.)

A major assumption made in the following analysis is that higher order modes of vibration of the beams do not play a significant role in the performance. This assumption is based on three factors: (1) it is unlikely that externally applied disturbance force frequencies high enough to excite higher modes will ever be encountered in a manufacturing context except in transient form, (2) the major disturbance forces will be present only at the end of the beam, and will thus tend to dominate forces generated along the beam's length, and (3) vibration of the structure induced by the joint servos will be bandlimited and also will not excite the higher modes significantly. It is reasonable to assume, therefore, that deflections caused by higher mode dynamics will be both small and short lived compared to first mode dynamics. Note also that since the actuator and measurement device are colocated, the problems commonly encountered in controlling the compliance of flexible structures are mitigated.

Allowing the first mode assumption, it is now possible to assume that all the mass is lumped at the end of each beam and is supported by a massless spring (Fig. 6). The effective mass for a cantilever beam can be obtained from:

$$M_{\text{eff}} = \int_0^L \frac{Y(x)m}{Y_{\text{end}}}\,dx + M_{\text{end}} \tag{1}$$

where

$L_{\text{eff}}$ = beam length
$Y(x)$ = vertical beam displacement
$x$ = position along the beam
$m$ = mass of beam per unit length
$Y_{\text{end}}$ = beam displacement at end
$M_{\text{end}}$ = any additional mass placed at the end

Unfortunately, $Y(x)$ is a function of the type of loading experienced by the beam. Even with the assumption of a single mode of vibration, the shape of the beam varies depending on the degree of dominance of the end force over the distributed acceleration force. The shape will vary between two extremes: (1) that which results from most mode vibration under no external end force, and (2) that which results from static bending under an end load. Rorak [6] gives the following expression for the frequency of first mode vibration:

$$f_n = -\frac{1}{2\pi}\left[(M_{\text{end}} + 0.236mL)L^3/3EI\right]^{-1/2} \tag{2}$$

where $EI$ is the bending rigidity. In order to find the effective mass, $M_{\text{eff}}$, that will produce this natural frequency in the

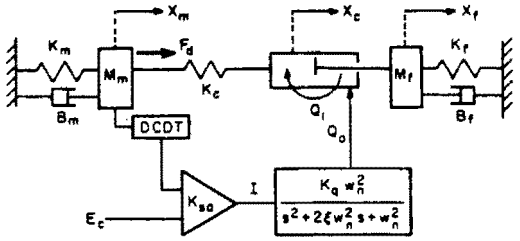


Fig. 7 Schematic of full system

lumped-mass model, it is necessary to find the effective spring constant, $K$, for a lumped mass cantilever. To do this, the equation governing beam end displacement, $Y_{\text{end}}$ for an end loaded beam, can be rewritten in terms of $K$:

$$K = M_{\text{eff}}/(gY_{\text{end}}) = 3EI/L^3 \tag{3}$$

This equation can be combined with the formula for natural frequency of a spring mass system:

$$f_n = (K/M_{\text{eff}})^{1/2}/2\pi \tag{4}$$

to form:

$$f_n = (M_{\text{eff}}L^3/3EI)^{-1/2}/2\pi$$

Comparing this equation to equation (2), it is evident that at the natural frequency the effective mass should be defined:

$$M_{\text{eff}} = M_{\text{end}} + 0.236\,mL \tag{5}$$

This compares to:

$$M_{\text{eff}} = M_{\text{end}} + 0.375\,mL \tag{6}$$

which is obtained by integrating equation (1) for the static case. Ideally, a frequency response analysis would use equation (5) at high frequencies and equation (6) at low frequencies, but since the difference is rather small for nonzero Mend, one value will be used. Rather than using the average of the two, equation (5) is chosen because of the need to keep the natural frequency as accurate as possible.

Although the compressibility of oil is usually fairly low, it can affect the higher frequency dynamics of the system. This effect is included in the model as a linear spring connecting the outer beam to the cylinder. The actual compressibility characteristics are linked with servovalve parameters and are non-linear, however, a linear model should give a reasonable approximation with the correct choice of spring constant.

As recommended by the valve manufacturer, a second order approximation is used for the servovalve transfer function. The frequency response of the second order model compares well with the actual response for frequencies up to 250 Hz, well past the fundamental frequencies of both beams. The model also includes provision for leakage flow in the valve.

A schematic of the system is shown in Fig. 7, which also defines the variables used in the model equations. Subscript m refers to the outer (moment carrying beam), $f$ to the inner (force carrying) beam, $K_c$ is the hydraulic oil stiffness, and $Q$ is the leakage flow.

The governing equations are derived here in terms of both the force disturbance input, $F_d$, and the control voltage input, $E_c$. Referring to Fig. 7, the following linear equations can be written from equilibrium on the two masses:

$$M_m\ddot{X}_m = -F_m + F_c - F_{bm} + F_d \tag{7}$$

$$M_f\ddot{X}_f = -F_c - F_f - F_{bf} \tag{8}$$

where:

$$F_m = K_m X_m \tag{9}$$

$$F_f = K_f X_f \tag{10}$$

and the hydraulic cylinder force

$$K_c = K_c(X_c - X_m) \tag{11}$$

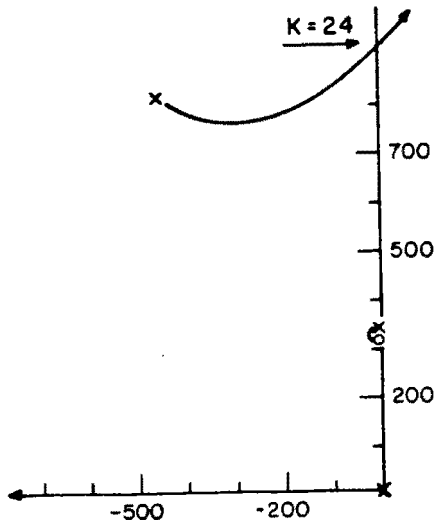


Fig. 8 Root locus for uncompensated system

For the hydraulic system, the governing equations are:

$$I = K_{sa}(E_c - K_{fx}X_m) \tag{12}$$

and

$$IK_q\omega_n^2 = \ddot{Q}_0 + 2\xi\omega_n\dot{Q}_0 + \omega_n^2 Q_0 \tag{13}$$

which is the second order servovalve characteristic. The leakage flow in the system is given by

$$Q_l = \frac{F_c}{A}K_{pg} \tag{14}$$

where $A$ is the cylinder area, and the flow delivered to the cylinder:

$$Q = Q_0 - Q_l \tag{15}$$

thus

$$Q/A = \dot{X}_c - \dot{X}_f \tag{16}$$

The system equations can be used to write state equations for this system, and the following were chosen as state variables:

$$Y1 = X_m$$

$$Y2 = d/dt(X_m)$$

$$Y3 = X_c$$

$$Y4 = X_f$$

$$Y5 = d/dt(X_f)$$

$$Y6 = Q_0$$

$$Y7 = d/dt(Q_0)$$

Equations (7)–(16) can now be rewritten in standard state matrix format:

$$\dot{\mathbf{y}} = A\mathbf{y} + B\mathbf{u} \tag{17}$$

and

$$X_m = C\mathbf{y} \tag{18}$$

The matrix equations (17) and (18) are closed-loop equations and will yield the closed-loop roots and frequency response. The open-loop characteristics can also be obtained from the state matrices if the feedback again, $K_{fx}$ is set to zero. The eigenvalues of $A$ will then yield the open-loop poles, and if $K_{fx}$ is then set to a very high value, a good approximation for the open-loop zero locations is obtained by again solving for eigenvalues of $A$. Any eigenvalues that do not become very large (i.e., moving toward infinity) are the open-loop zeroes. (The system described here consists of seven poles and five zeros.) The actual parameters used were made on the prototype and taken from manufacturers data. A table of these values is included in the Appendix.

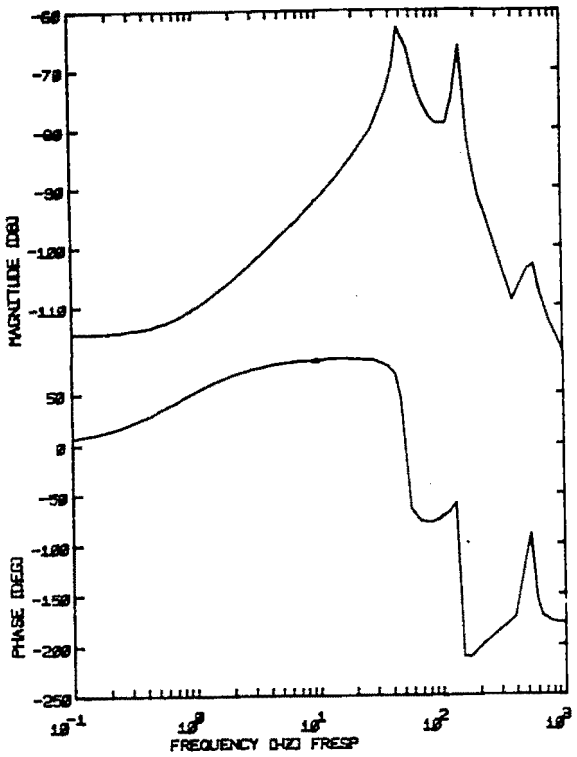


Fig. 9 Closed-loop bode plot – uncompensated

The output of the second order servovalve model was defined to be fluid flow volume, and the assumption mode here was that flow is proportional to the displacement of the valve spool, regardless of load or amplitude. This is a commonly made assumption and holds up quite well as long as loads stay within approximately 50 percent of maximum and signal amplitude stays within the valve rating.

Initially, proportional control was investigated. It was found that because of high frequency noise, the amplified DCDT output required low-pass filtering to avoid saturating the amplifier. However, the break frequency of the filter was kept sufficiently high (400 Hz) to avoid affecting system dynamics significantly. The following response data was calculated for the system without a filter. The closed-loop roots were obtained, for various values of proportional gain for the amplifier. The resulting root locus, shown in Fig. 8, indicates a maximum allowable gain of 24 ma/volt. (Two of the seven roots are very fast and are omitted.) The closed-loop Bode diagram of system disturbance response near this maximum gain is shown in Fig. 9. In this case, the input is disturbance force and the output is beam displacement, thus the magnitude represents the displacement, in inches, divided by the input force in pounds. For example: – 100 dB indicates that the beam moves 0.001 cm under a load of 100 Newtons.

Note that the static displacement magnitude is small but definite, as indicated by the leveling off of the curve as the frequency approaches zero. This is in spite of the integrating action of the actuator and is caused solely by non-zero open loop pole near the origin. The size of the static error, however, is inversely proportional to the gain of the amplifier and, in the case, is effectively zero as the magnitude plot shows. Using the −100 dB magnitude response of the previous example as a performance goal, Fig. 9 also shows that the proportionally controlled system, at maximum gain, can be expected to achieve this goal for all disturbance frequencies below 4 Hz.

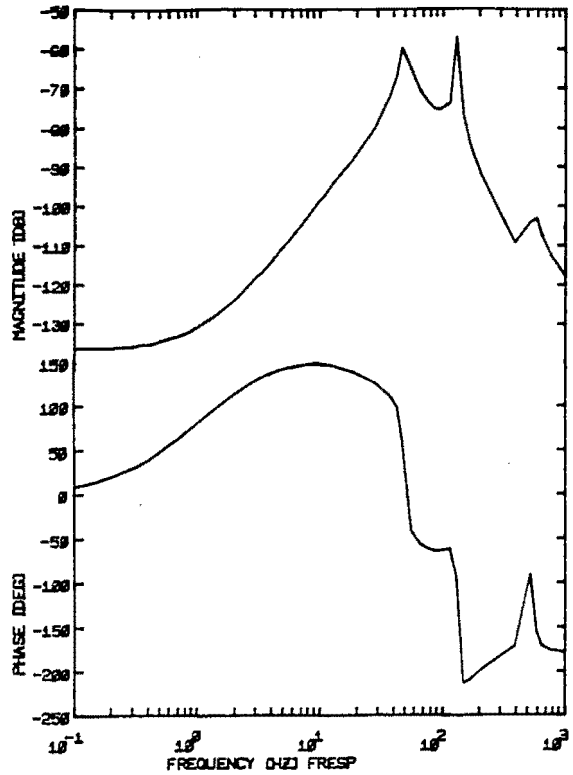


Fig. 10 Closed-loop bode plot – compensated

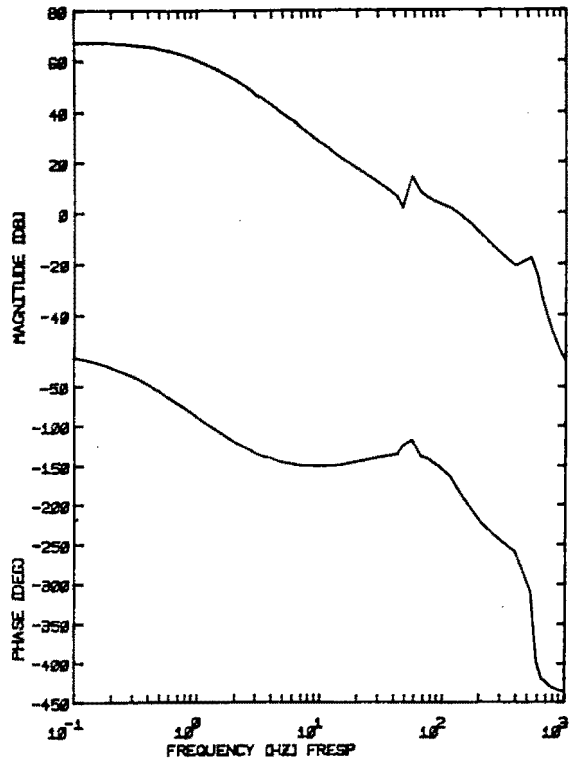


Fig. 11 Open-loop bode plot – compensated

## Compensator Design

The type of controller ultimately used for experimentation, unfortunately, had to take into consideration the properties of the DCDT signal. The DCDT produced a d-c voltage, but with a superimposed 4000 Hz square wave signal and this a-c signal, when amplified, saturated the servoamplifier in both directions. It was found that the signal required a ten-fold reduction in amplitude to avoid amplifier saturation. Partly for this reason, a lag compensator was chosen.

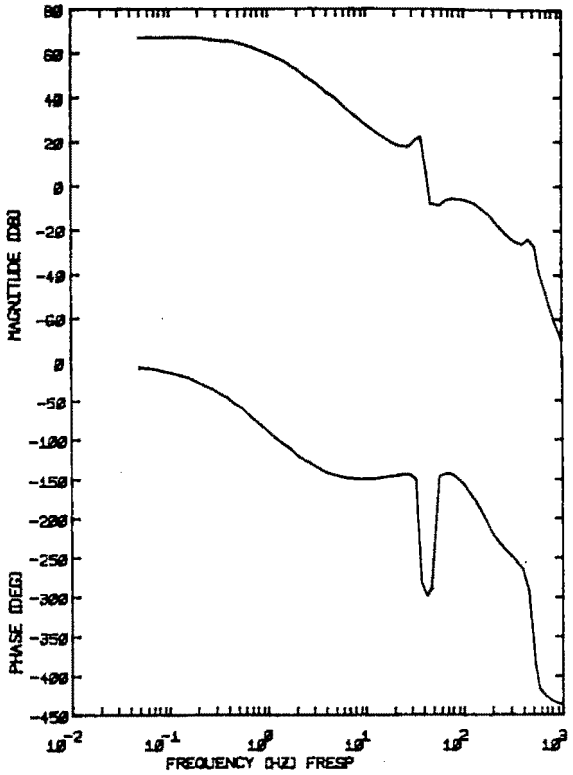


Fig. 12 Open-loop bode plot for system with high end-mass – unstable

The lag compensator allowed a higher d-c gain to be used, but it reduced the system gain at higher frequencies to levels that prevented a-c saturation from the DCDT. It was found by pole placement analysis that the greatest improvement could be made by using break frequencies of 1.75 Hz and 26 Hz for the pole and zero respectively. The resulting frequency response curve (Fig. 10) shows a 22 dB improvement in performance below 2 Hz, a 20 to 4 dB improvement between 2 Hz and 20 Hz, and no improvement above 25 Hz as expected.

In this case the $-100$ dB goal is achieved for all disturbance frequencies below 10 Hz, with a static error of approximately 0.00085 cm under a 100 Newton load.

## Effect of a Load Mass

Thus far, the system performance under force disturbance has been studied. In order to make the system truly adaptable to robots each link must be able to handle such disturbances while supporting the mass of object, as well as the mass of other links attached onto its end, if any. The end mass is a critical parameter to system stability with the present controller, as can be seen by examination of the open-loop response (Fig. 11). Note the peaks at 50 Hz and 55 Hz. Clearly one is caused by a complex pole while the other is caused by a complex zero. In fact, the pole corresponds to the natural frequency of the outer beam while the zero is at the natural frequency of the inner beam. More importantly, the pole frequency is higher than that of the zero. The significance of this fact can be seen on the phase response curve, where the net effect of the two resonances is a phase spike in the positive direction. If the order of the zero-pole pair were reversed, this spike would be in the negative direction and would result in instability with the gain indicated (see Fig. 12). Such reversal is, in fact, not only possible, but quite likely since the natural frequency varies as the inverse square root of the end mass,

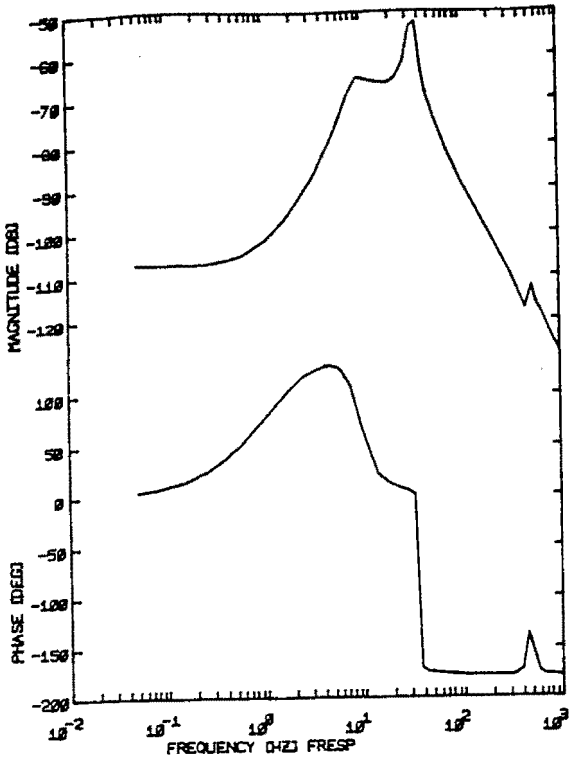


Fig. 13 Closed-loop bode plot for system with high end-mass at maximum stable gain

and any additional end mass will be placed on the outer (pole) beam. If the reversal were to take place, the crossover frequency would become the natural frequency of the outer beam and would necessitate an immediate 75 percent reduction in amplifier gain to achieve stability. Further increase in end mass would call for progressively lower gain. Fig. 13 shows the closed-loop response with a 6.8 Kg end mass and the corresponding maximum gain. The gain is 30 times lower than the maximum gain without extra end mass.

The end mass problem can be overcome in many ways, for example: (1) The stiffness of the outer beam can be increased to push the complex pole frequency higher. (2) The frequency of the zero can be decreased to put it ahead of the pole at all times. (This can be done by decreasing the inner beam's stiffness, increasing its end mass, or both.) (3) Redesign of the controller to provide additional phase below 50 Hx such that the open-loop phase spike does not cross $-180$ with beam end mass at a maximum. (4) Use parameter adaptive control to ensure global stability.

Because of easy implementation for experiments, option (2) was considered here. Figure 14 shows the frequency response of the same system but with a 4.5 Kg mass placed at the end of the inner beam to avoid zero-pole reversal. This allowed the gain to be raised from 10 to 200, with a similarly dramatic improvement in performance. As the figure shows, performance is better than $-100$ dB up to 8 Hz.

Since the linear model does not account for the pressure dependent servovalve characteristics, the different piston areas presented by the single sided cylinder and the possibility of air in hydraulic fluid, a series of simulations were performed with these non-linear factors accounted for. The conclusions from these simulations (see [5] for details) are:

(1) The maximum gain and the maximum load are governed by the smaller of the two piston areas, rather than the average, and

(2) The amplitude of response is accurately predicted by the linear model as long as loads stay moderate, and the oil is kept air free.

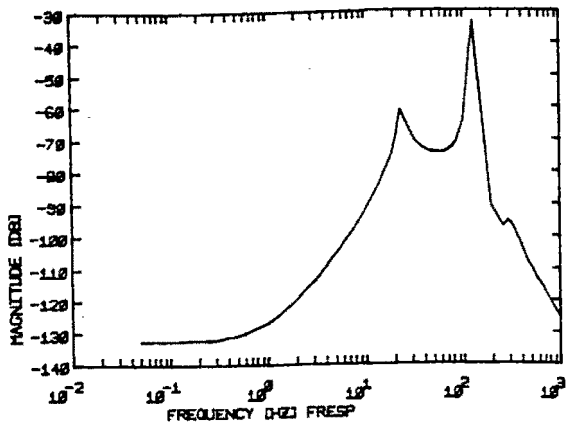


Fig. 14 Closed-loop bode plot for high-mass system with mass compensation

## Experiments

The system described above was constructed to allow dynamic response tests to be performed. The beam system was mounted on a rigid foundation (a pressbrake frame) and feedback measurements made with DCDT.

The stability limit for the proportional control system with a lowpass filter at 400 Hz on the DCDT signal was found to be:

$$K_{sa} = 15 \text{ ma/volt versus } 24 \text{ predicted by linear model.}$$

The difference was assumed to be caused in part by a slight reduction in crossover frequency caused by the low-pass filter, and by the effect of the smaller area on one side of the piston. A lag compensator was then implemented according to the design described above. The gain at the point of instability was found to be:

$$K_{sa} = 200 \text{ ma/volt versus } 300 \text{ predicted.}$$

To check the effect of the complex pole-zero reversal, a 6.8 Kg mass was placed on the outer beam and the maximum gain was:

$$K_{sa} = 7 \text{ ma/volt versus } 10 \text{ predicted.}$$

One of the methods proposed to deal with the high end mass was the lowering of inner beam natural frequency by increasing its end mass. This was done by putting a 4.4 Kg mass at the end of the inner beam. The result was:

$$K_{sa} = 150 \text{ ma/volt versus } 200 \text{ predicted.}$$

Dynamic disturbance forces were then created using springs and masses to produce a sinusoidal input, which could be compared directly with the predicted response at a given frequency. These disturbance forces range in amplitude from 50 to 500 N(peak-peak) and had frequencies ranging from 0 to 10 Hz. The results are shown in Fig. 15, plotted on the frequency response curve obtained from the model. The phase of the output relative to the input was not measured for each point, but examination of oscilloscope traces verfied the predicted phase lead.

The same set-up was used to test the high mass response, with a 6.8 Kg mass placed on the outer beam's end, and a 4.5 Kg mass placed inside the inner beam's end. A more limited set of tests were performed and the results plotted on the corresponding predicted frequency response curve (Fig. 16).

In general, the test results agreed well with the predicted values. The lower value of measured critical gains is most probably caused by the unequal pistion areas which have the effect of changing the system gain depending upon the flow direction. As the results show, effectiveness of the bending load rejection was considerable better at low frequencies (0 to 10 Hz) than at the intermediate frequencies (10-100 Hz). At

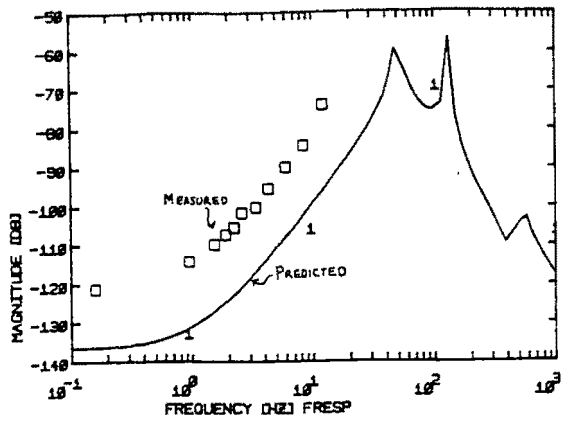


Fig. 15 Actual frequency response versus predicted low end-mass, with lag controller

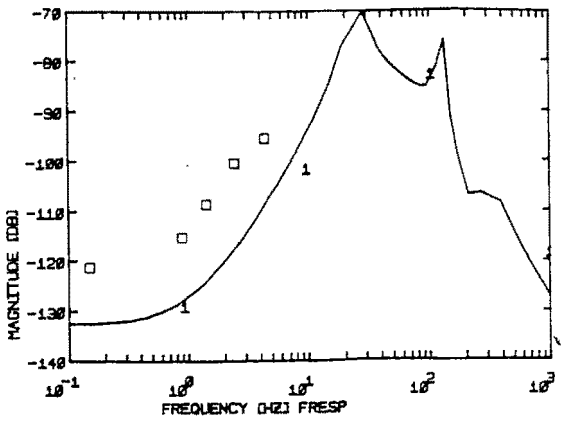


Fig. 16 Actual frequency response versus predicted high end-mass, mass compensated

high frequencies the results shown bending is again very minimal.

The performance at low frequencies was quite good. In fact, for frequencies below 2 Hz, accurate measurements of beam displacement were so small that they were overshadowed by system noise. The equipment used for measuring displacement had resolution to approximately 0.005 mm, so reduction of bending was limited to this value, whereas predicted static error was as low as 0.0005 mm per 100 N load. On the other hand, reduction of bending past $-110$ dB is of little use since other errors in the system invariably exceed this value.

## Conclusions

The use of active deflection compensation has been addressed as a means of improving manipulator precision. It obviates complex and costly end point position and orientation measurement, but introduces several new servo systems to the basic machine. However, these servos act independent of the joint servos and can, therefore, be considered autonomous subsystems. Also, in actual practice a pair of orthogonal bending deflection compensators would be required and the effect of apparent bending error caused by torsion in the beam must still be addressed.

It is worthwhile noting that although the goal here was to reduce the deflections caused by bending, which translates to desiring an extremely low bending compliance, the same control system (through the use of variable gains, for example) can be used to actively increase or vary dynamically the compliance of the beam to suit interactive assembly tasks.

Although the twin-beam deflection compensation design can be made to work in its present state of development, the classical control methods employed here can be much improved on by the use of state variable feedback methods. Using such methods, which would most likely call for a greater number of sensors and/or state observation, the performance of the beam can be made as near perfect as the power available will permit, limited, however, by the single mode beam approximation.

## Acknowledgments

This work was supported in part by a Hughes Fellowship and the Ralph Cross Lectureship at MIT. The loan of servovalve equipment by Moog, Inc. is also gratefully acknowledge. Ms. Paula Suvanto is responsible for the actual production of this document.

## References

1 General Dynamics, Fort Worth, "Robotic Systems for Batch Manufacturing—Task A," USAF Contract F33615-78-5188 (ICAM Program).

2 Book, W. J., "Characterization of Strength and Stiffness Constraints on Manipulator Control," *Theory and Practice of Robots and Manipulators*, Morecki Dedzior (eds.), 1976.

3 Kratkiewicz, G. L., "Automatic Control of a Micromanipulator to Improve Manipulator Position Accuracy," S. B. thesis, Department of Mechanical Engineering, MIT, May 1982.

4 Van Devegte, J., and Hladun, A. R., "Design of Optimal Passive Beam Vibration Controls by Optimal Control Techniques," ASME JOURNAL OF DYNAMIC SYSTEMS, MEASUREMENT AND CONTROL, Vol. 95, No. 4, 1973, pp. 427–434.

5 Zalucky, A. D., "Reduction of Beam Bending Using Active Compliance Control—A New Design," S. M. thesis, Department of Mechanical Engineering, MIT, May 1982.

6 Roark, R. J., and Young, W. C., *Formulas for Stress and Strain* 5th Edition, McGraw-Hill, New York, 1975, p. 576.

## APPENDIX

From measurements made on the prototype and from manufacturer's data, the following parameter values were obtained:

| | |
|---|---|
| Outer beam spring constant | $K_m = 4868$ N/cm |
| Inner beam spring constant | $K_f = 1575$ N/cm |
| Beam structural damping | $\zeta = 0.05$ |
| Oil spring constant | $K_c = 130{,}000$ N/cm |
| Outer beam effective mass | $M_m = 3.9$ Kg |
| Inner beam effective mass | $M_f = 1.6$ Kg |
| Servovalve flow gain (6.9 MPa) | $K_q = 11.3$ cm$^3$/s/mA |
| Servovalve pressure gain | $K_p = 29.6$ MPa/mA |
| Servovalve leakage gain | $K_{pq} = 3.8 \times 10^{-7}$cm$^3$/s/Pa |
| Servovalve natural frequency | $f_n = 150$ Hz |
| Piston area (ave.) | $A = 1.13$ cm$^3$ |
| DCDT + op-amp gain | $F = 11.8$ volts/cm |